International Journal of Thin Films Science and Technology

http://dx.doi.org/10.18576/ijtfst/150108

Thermally Induced Structural Changes and Optical Properties of $(ZnSe)_{0.9}Cu_{0.1}$ Chalcogenide Thin Films

Mahmoud N. Abdel-Salam [1], *N. Sabry* [2], *M. S. I. Koubisy* [1], *E. R. Shaaban* [1,*]

[1]Department of Physics, Faculty of Science, Al-Azhar University, Assiut 71542, Egypt
[2]Nanoscience Laboratory for Environmental and Biomedical Applications (NLEBA), Nuclear Lab., Department of Physics, Faculty of Education, Ain Shams University, Roxy, 11757 Cairo, Egypt

Received: 12 Jun. 2025, Revised: 3 Dec. 2025, Accepted: 8 Dec. 2025
Published online: 1 Jan. 2026

Abstract: $(ZnSe)_{0.9}Cu_{0.1}$ nanocrystalline thin films were deposited by the thermal evaporation technique. Then, annealed in the temperature range from 100 °C to 500 °C. The microstructural and optical properties of as-deposited and annealed films were investigated by XRD diffraction analysis techniques and UV–Vis spectrophotometer, respectively. The crystallite size of the investigated films exhibited a unique phase of wurtzite hexagonal structure with no other phases and increased with increasing annealing temperatures, while the strain and dislocation density decreased. Optical properties exhibited a blue shift effect, and the optical band gap was increased from (2.527 to 2.659 eV), whereas the Urbach energy decreased from (0.341 to 0.133 eV) as annealing temperatures increased. The steepness parameters and electron-phonon interactions are calculated. The single oscillator model Wemple–Didomenico was used to calculate the dispersion parameters of $(ZnSe)_{0.9}Cu_{0.1}$ thin films. In addition, some optical parameters as single oscillator energy E_o, the dispersion energy E_d, the average oscillator strength s_o, the ratio of carrier concentration N/m^*, plasma frequency ω_p, and dielectric constant ε_r are examined. Finally, the non-linear optical parameters are identified and affected by increasing the annealing temperatures.

Keywords: $(ZnSe)_{0.9}Cu_{0.1}$; annealing temperature; thin films; X-ray diffraction; microstructural parameters; optical properties.

1 Introduction

Semiconducting compounds are made up of elements from groups II (metals) and VI (chalcogens) of the periodic table. These semiconducting materials have garnered significant interest in both scientific research and practical applications. Furthermore, materials with a high chalcogen element content are frequently utilised in memory and switching devices, such as electrochemical sensors, solar cells, integrated optics, electrophotography, optoelectronics, and devices for optical and electrical memory [1,2,3]. Thin films of chalcogenide glass semiconductors (ZnSe) have garnered interest because of several comparable physical and chemical characteristics as a higher refractive index, high electrical conductivity, strong optical transmission in the visible and infrared wavelength range, and a direct band gap II-VI group (2.7eV) at room temperature [4,5]. These properties can be improved by altering the growth parameters—such as dopant concentration, pH, deposition method[6]. In addition, ZnSe thin films cover many applications, including optoelectronic devices such as blue-green lasers, light-emitting diodes, optically controlled switches, dielectric mirrors and filters, solar cells, and infrared optical devices[7,8,9,10]. Copper is one of the important transition metals that can be doped with ZnSe to make a ternary alloy system due to its relative ionic radius with Zn [11]. The small size and electronegativity differences between metals and chalcogens, the formation of chalcogen-to-chalcogen bonds, and the possibility of metal-metal bonding within the structure allow for a wide range of stoichiometry and crystal structures, as well as the resulting functional properties. Their charge and heat transport characteristics are influenced by the high concentration of defects, which has a significant impact on their electrical, thermoelectric, and optoelectronic characteristics[12]. Particularly, by enhancing the characteristics, increasing the range of absorption spectrum, and narrowing its energy band-gap, which leads to an increase in the photo-absorption coefficient[13,14]. In addition, owing to these properties, many methods are used to fabricate pure and doped ZnSe polycrystalline thin films as “the spray-pyrolysis technique”,

* Corresponding author e-mail: esam_ramadan2008@yahoo.com

"pulsed laser deposition" "thermal evaporation technique", "magnetron sputtering", and "chemical bath deposition" ...etc [15,16,17,18]. The thermal evaporation technique is a good method, due to its low cost, repeatability, and adaptability to deposition on a large substrate area. The films produced using this method are also exceedingly uniform and highly adhesive [19].

Our most recent published study evaluates and reports the effect of Cu inclusion on the optical properties of ZnSe thin films [20]. The main goals of this paper are to assess the impact of annealing temperatures on the optical, structural, and compositional linear and non-linear parameters of $(ZnSe)_{0.9}Cu_{0.1}$ thin films by using X-ray diffraction and UV–Vis spectrophotometer in the range between 300 to 2400 nm of wavelength. Relative linear and non-linear optical parameters match structural parameter data, offering important insight into how to maximize the performance of such materials in optical and electrical devices.

2 Experimental procedure

The melt-quenching method was used to fabricate the bulk alloys of $(ZnSe)_{90}Cu_{10}$ from 99.999% pure materials (Aldrich Chem Co., USA), utilising the necessary atomic ratio quantities of Zn, Se, and Cu elements after a 24-hour annealing process at 1400 K in an oscillating furnace. In the earlier paper, the previous inquiry approach was mentioned [20]. The films were deposited on highly cleaned substrate glasses employing a coating unit (DV-502A; Denton Vacuum, Cherry Hill, NJ, USA) at a vacuum of 10^{-7} mbar in a thermal evaporation machine. The temperature of the substrates was adjusted to 300 K with a rate of deposition of 10 Å/sec during the preparation of thin films. The thickness of the fabricated films is 500 nm. Then, the films are annealed from 100 °C to 500 °C in a muffle furnace. XRD diffraction apparatus with the Cu Kα ($\lambda = 1.54016$ Å) radiation using the X-ray mechanism "XRD Philips 1710" was used to analyze the microstructure properties of as-prepared and annealed films, and a UV–Vis spectrophotometer in the range between 300 to 2400 nm was applied to investigate the optical properties of the synthesized films.

3 Results and discussion

3.1 XRD and microstructural studies

The XRD diffraction of as-prepared and thermally annealed $(ZnSe)_{0.9}Cu_{0.1}$ thin films from 100–500 °C is illustrated in Fig. 1. The crystalline phases revealed that all thin films have a unique polycrystalline wurtzite hexagonal (ZnSe) structure with space group $P6_3mc$. The lattice constants of annealed films are in agreement with the standard values of ZnSe thin film, $a = 3.9960$ Å and $c = 6.55$ Å, reported in ICSD Card 00-015-0105 [20]. Without the appearance of another phase of Zn, Se, and Cu with increasing annealing temperature, due to the good crystallinity of the thin films with Cu ions incorporated in the ZnSe lattice [21]. Additionally, in Fig. 1, one can see that as the annealing temperature increases, the main diffraction planes (002), (110), and (112) for ZnSe phase become sharper and the intensity of the diffraction patterns increases, indicating an enhancement in the crystallization process as a function of annealing temperature [22,23].

Furthermore, it was noted that as the annealing temperature rose, the location of the preferred diffraction peaks changed. Additionally, as Fig. 2 illustrates, the broadening (FWHM) of diffraction patterns decreases with increasing annealing temperature, revealing that the development of crystallinity causes an increase in peak intensity. This suggests that as the annealing temperature increases, the thermal annealing process releases energy for atoms to diffuse, causing crystallites to grow and rearrange. Initial strain may result from the addition of Cu to the ZnSe lattice, but this strain is relieved by annealing [24,25].

By using Bragg's equation with the following formula [26], the interplanar spacing d at the first order approximation ($n = 1$) of the main diffraction plane (002) of the investigated films is estimated and listed in table 1:

$$d = \frac{\lambda}{2\sin\theta} \tag{1}$$

Additionally, the lattice constants a, c, and the unit cell volume V for the as-prepared and annealed films are evaluated by the formulas as described below [26]:

$$a = \frac{\lambda^2}{\sqrt{3}\sin\theta} \tag{2}$$

$$c = \frac{\lambda}{\sin\theta} \tag{3}$$

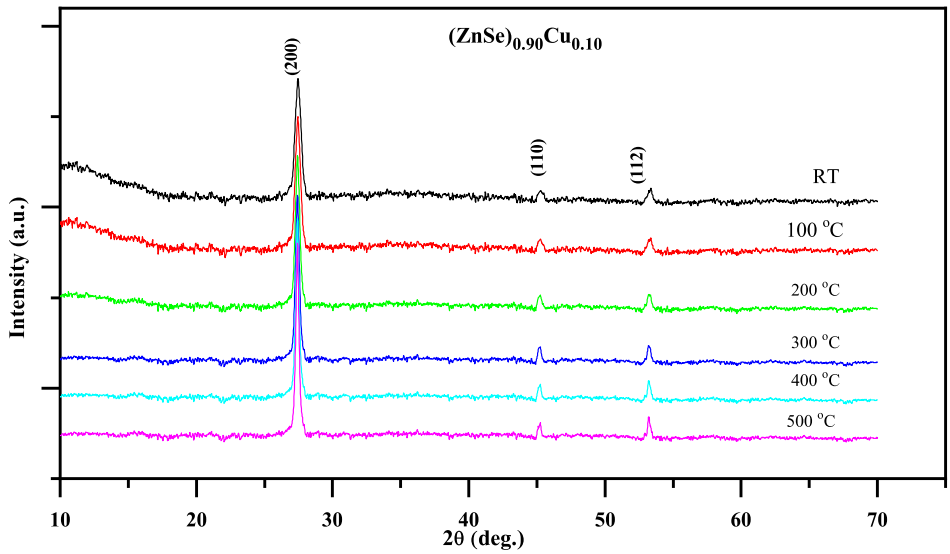

Fig. 1: The XRD graph as a function of annealing temperatures of $(ZnSe)_{0.9}Cu_{0.1}$ thin films.

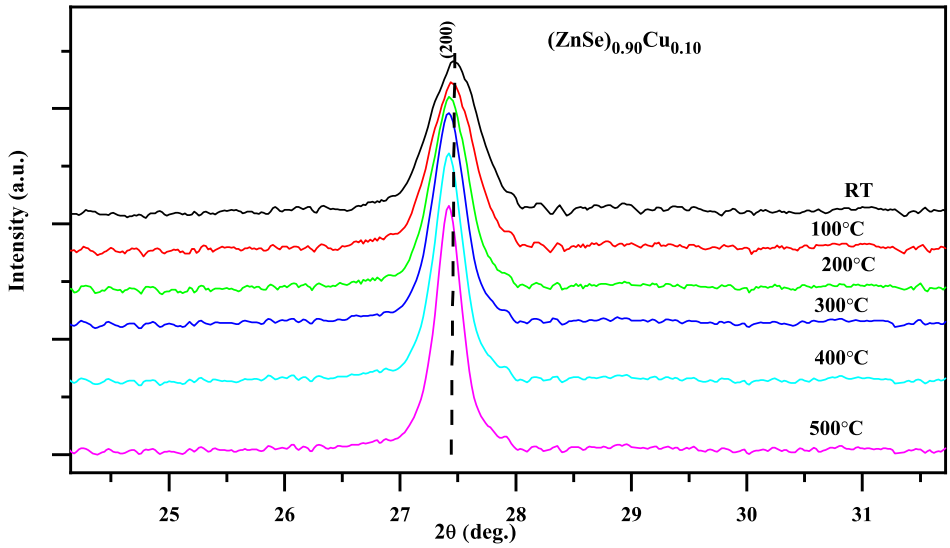

Fig. 2: The change in the peak shift of the (002) plane of the annealed $(ZnSe)_{0.9}Cu_{0.1}$ thin films.

$$V = \frac{\sqrt{3}}{2}a^2c \tag{4}$$

By comparing the measured d_H-value indicated from XRD data with the standard d-values, the relative percentage error is estimated using the formula as shown below [27]:

$$\text{Relative} - \text{percentage} - \text{error} = \frac{d_H - d}{d} \times 100\% \tag{5}$$

To more understanding of the internal structural changes of the investigated films, the dependency of the lattice constant, unit cell volume, and other lattice parameters is calculated and tabulated in table 1. it's clear that the lattice parameters a, c, and interplanar spacing (d-spacing) are changed and increase slightly with increasing annealing temperature from (RT- 300 C°) due to the lattice expansion while all three parameters are constant from (400 to 500 C°),

Table 1: Some of the structural and lattice parameters of as-prepared and annealed $(ZnSe)_{0.9}Cu_{0.1}$ thin films.

Temp. (°C)	a (nm)	c (nm)	c/a	V (Å^3)	d-spacing (nm)	Lorentz-factor	Lorentz polarization factor	Relative % error
RT	0.3735	0.6316	1.6908	76.3153	0.3244	4.561	32.6271	-0.181
100	0.3749	0.6328	1.6881	77.0225	0.3247	4.572	32.6874	-0.092
200	0.3752	0.6339	1.6898	77.2690	0.3249	4.578	32.7391	-0.030
300	0.3753	0.6344	1.6903	77.3766	0.3250	4.581	32.7648	0
400	0.3753	0.6346	1.6908	77.3986	0.3250	4.581	32.7644	0
500	0.3753	0.6346	1.6908	77.3969	0.3250	4.580	32.7639	0

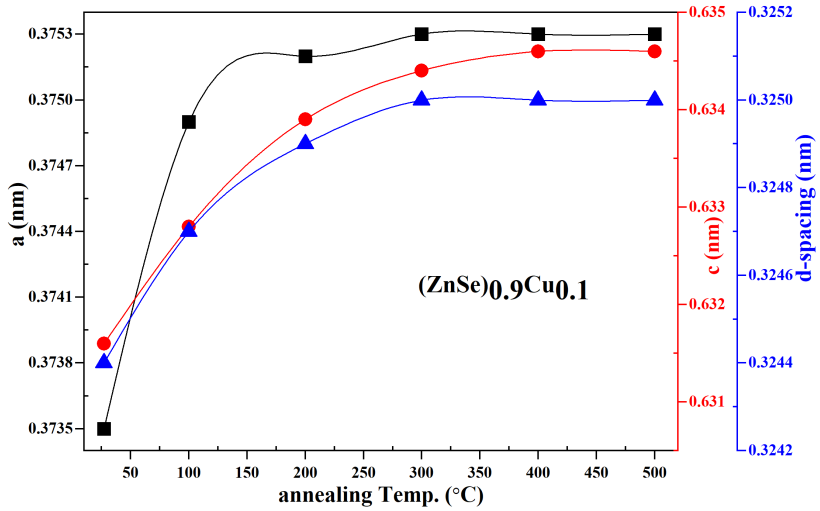

Fig. 3: Dependence of lattice parameters a, c, and d-spacing of as-prepared and annealed $(ZnSe)_{0.9}Cu_{0.1}$ thin films.

see Fig. 3. in addition, the values of relative percentage error equal zero for annealed thin films from (300-500 C°) due to clos of the calculated value of d- spacing with standard d- value (0.325 nm). These results prove that improved crystallinity and reduced disorder in all films under study occur with increasing annealing temperature [23]. further, as the annealing temperature progressed from RT to 500 C°, the cell volume grew from 76.3153 to 77.3969 $A^{\circ 3}$. By incorporating Cu^+ ions (ionic radius ≈ 0.74 Å) into Zn^{2+} sites and thermally relaxing intrinsic strain, this anisotropic expansion reduces lattice distortion and improves the stable wurtzite structure of ZnSe thin films with a ratio of $(c/a = 1.69)$[28].

The Lorentz factor and Lorentz polarization factor are evaluated by equations below, then listed in table 1. From these results, the values of the Lorentz factor and Lorentz polarization factor are slightly increasing with increasing annealing temperature due to a shift in 2θ to low values with increasing annealing temperature.

$$\text{Lorentz-factor} = \frac{\cos\theta}{\sin^2 2\theta} = \frac{1}{4\sin^2\theta\cos\theta} \tag{6}$$

$$\text{Lorentz-polarization-factor} = \frac{1+\cos^2 2\theta}{\sin^2\theta\cos\theta} \tag{7}$$

The important microstructural variables, such as crystallite size, lattice strain, dislocation density, and number of crystallite sizes per unit surface, were determined from XRD reflectance data, using the equations described below. The Debye–Scherrer equation was used to calculate the crystallite size (D) of the films [29].

$$D = \frac{K\lambda}{\beta\cos\theta} \tag{8}$$

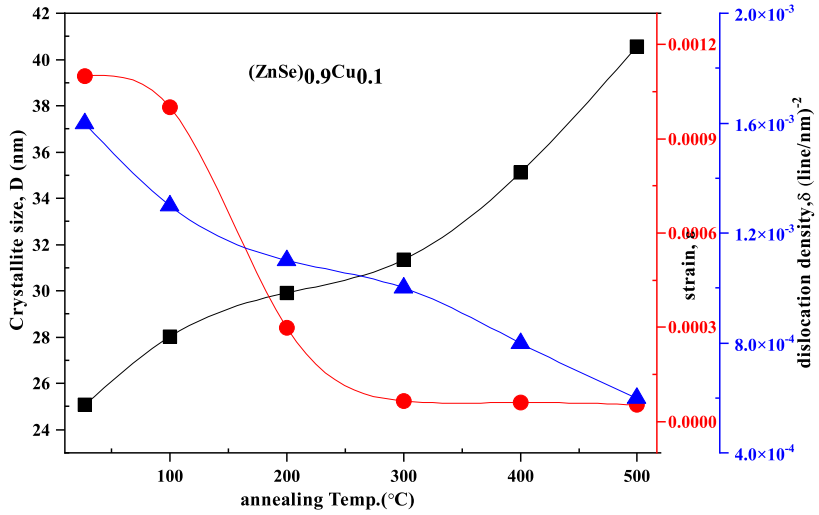

Fig. 4: The changes of crystallite size D, lattice strain ε, and dislocation density δ of $(ZnSe)_{0.9}Cu_{0.1}$ films as a function of annealing temperatures.

Here, the wavelength of the Cu Kα XRD source is 1.54056 Å, λ is the Bragg's diffraction angle, β is the corrected full width at half maximum (FWHM) at the intensity peak, and k is a constant at 0.94. The lattice strain (ε), which represents the degree of disorder in the lattice of films, was estimated using the following formula [29].

$$\varepsilon = \frac{\beta}{4\tan\theta} \tag{9}$$

Moreover, the dislocation density (δ) and the number of crystallites per unit surface (N_C) were calculated by the formula as shown below [30].

$$\delta = \frac{1}{D^2} \tag{10}$$

$$N_C = \frac{d}{D^3} \tag{11}$$

The changes of crystallite size, lattice strain, and dislocation density as a function of annealing temperature are depicted in Fig. 4. From these results, the crystallite size (D) increases while lattice strain (ε) and dislocation density (δ) decrease. The increase in crystallite size may be due to the indication of grain growth facilitated by enhanced atomic mobility at elevated temperatures, which led to good crystallinity of films [31]. On the other hand, a large decline in lattice strain and dislocation density below the annealing temperature of 300 °C was caused by annihilation of point imperfections, dislocation recombination, and dislocations migrating to grain boundaries or annihilating with increasing annealing temperature [32,33]. In addition, the number of crystallites per unit surface decreases with increasing annealing temperature. This result may be due to secondary recrystallization involving Ostwald ripening, which causes subcritical grains to shrink and vanish, leading to a bimodal size distribution and reduced grain density. Additionally, the process of diffusion-controlled ripening leads to the growth of large grains at the expense of small ones [31,34,35]. The values of the above-mentioned parameters are listed in table 2.

The positional parameter u and the length of the bond, l, of the wurtzite structure are computed by the formulas described below [36] and presented in table 3.

$$l = \sqrt{\frac{a^2}{3} + c^2\left(\frac{1}{2} - u\right)^2} \tag{12}$$

Where u is described as just a positional parameter of the wurtzite structure, obtained by

$$u = \frac{a^2}{3c^2} - 0.25 \tag{13}$$

Table 2: The microstructural parameters of the studied $(ZnSe)_{0.9}Cu_{0.1}$ thin films annealed at different temperatures.

Temp. (°C)	D (nm)	$\varepsilon \times 10^{-5}$	$\delta \times 10^{-3}$ (lin/nm)$^{-2}$	$N \times 10^{-2}$ nm^{-2}
RT	25.084	110	1.6	3.17
100	28.013	100	1.3	2.30
200	29.911	29.71	1.1	1.80
300	31.355	6.54	1.0	1.60
400	35.120	6.01	0.8	1.10
500	40.566	5.26	0.6	0.70

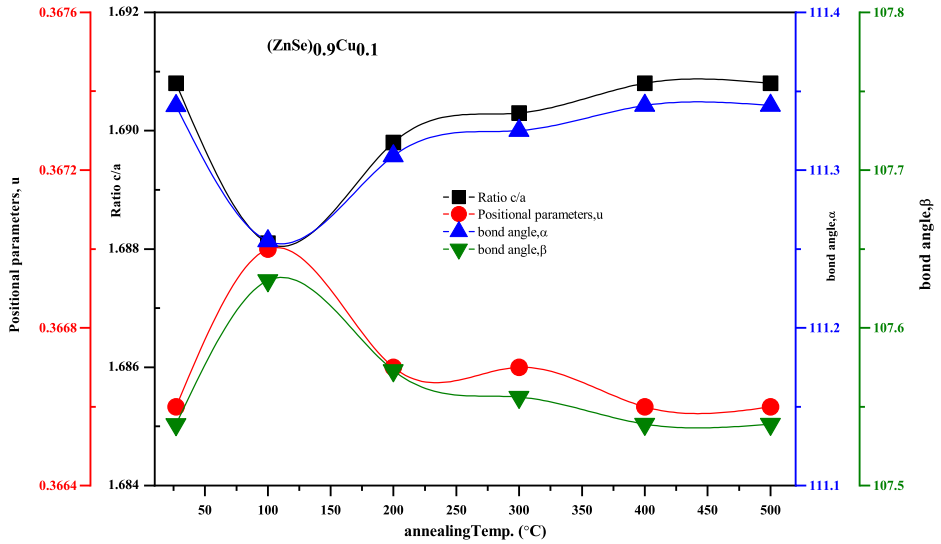

Fig. 5: Ratio c/a, positional parameter and bond angles, α, β for as-prepared and different annealed $(ZnSe)_{0.9}Cu_{0.1}$ thin films.

The 2nd-nearest neighbors and bond angles, α, β, can be estimated by the following equations [26,37].

$$b_1' = c(1-u) \tag{14}$$

$$b_2' = \sqrt{a^2 + (uc)^2} \tag{15}$$

$$b_3' = \frac{4}{3}a^2 + c^2\left(\frac{1}{2} - u\right)^2 \tag{16}$$

$$\alpha = \frac{\pi}{2} + \cos^{-1}\left[1 + 3\left(\frac{c}{a}\right)\left(-u + \frac{1}{2}\right)^2\right]^{-1/2} \tag{17}$$

$$\beta = 2\sin^{-1}\left[\frac{4}{3} + 4\left(\frac{c}{a}\right)^2\left(-u + \frac{1}{2}\right)^2\right]^{-1/2} \tag{18}$$

From the results listed in table 3, the deviation of the positional parameter, u, indicates a distortion in the c-direction. The observed $u < 0.375$ suggests that the bonds along the c-axis are compressed with increasing annealing temperature. Additionally, the bond lengths (l, b_1', b_2', b_3') increase, indicating lattice relaxation. The increase in bond lengths is due to the reduction of defects and strain [32,33], and also the incorporation of Cu atoms. Cu^{+} has a similar ionic radius to Zn^{2+} (0.74 Å for both in tetrahedral coordination, so the substitution does not cause major distortion, but the difference in charge and bonding may lead to subtle changes [20,26]). On the other hand, Fig. 5 describes the relation between

bond angles α, β, positional parameters u, and ratio of c/a. The bond angles α and β are both deviated from the ideal tetrahedral angle (109.47°). The calculated values of as-prepared and annealed thin films are typical for wurtzite II–VI compounds. The distortion is due to the ionic nature and the difference in the c/a ratio from the ideal ($c/a = 1.633$) [38]. In our study, the c/a ratio was around 1.69, which is higher than ideal, leading to an elongated c-axis. This elongation is consistent with the observed bond angles ($\alpha > \beta$). The stabilization of the parameters from 400°C to 500°C indicates that the material reaches a stable configuration.

Table 3: Potential parameter, bond length, nearest neighbor bond length, and both bond angles for $(ZnSe)_{0.9}Cu_{0.1}$ thin films annealed at different temperatures.

Temp. (C°)	u	L (Å)	b_1' (Å)	b_2' (Å)	b_3' (Å)	α (°)	β (°)
RT	0.3666	0.2315	0.4000	0.4395	0.4395	111.3407	107.5388
100	0.3670	0.2322	0.4006	0.4410	0.4410	111.2550	107.6300
200	0.3667	0.2325	0.4015	0.4414	0.4414	111.3090	107.5730
300	0.3667	0.2326	0.4018	0.4415	0.4415	111.3250	107.5560
400	0.3666	0.2326	0.4019	0.4415	0.4415	111.3410	107.5390
500	0.3666	0.2326	0.4019	0.4415	0.4415	111.3410	107.5390

3.2 Optical Properties

3.2.1 Transmittance, Absorption Coefficient, and Band Gap Calculations

The optical band gap energy from band-to-band transition mechanisms in semiconductor thin films is related to the absorption coefficient, α. The following expression can be used to estimate the absorption coefficient, α [39], depending on the measured data of R_λ and transmittance T_λ spectra:

$$\alpha = \frac{1}{d} \ln \left[\frac{(1-R_\lambda)^2 + \sqrt{(1-R_\lambda)^4 + 4(T_\lambda R_\lambda)^2}}{2T_\lambda} \right] \tag{19}$$

where d is the film thickness. The calculated values of the optical parameters, such as reflectance R_λ and transmittance T_λ, as a function of the wavelength spectrum range between 300 to 2400 nm for as-prepared and annealed $(ZnSe)_{0.9}Cu_{0.1}$ thin films, are illustrated in Fig. 6. All of the deposited films clearly showed good transmittance in the visible region; the transmittance T_λ increased as the annealing temperature rose, reaching almost 85% for the film annealed at 500 C°.

In contrast, the reflectance R_λ exhibits the opposite tendency, decreasing with increasing annealing temperature. These trends may be attributed to the improvement of crystallinity with increasing annealing temperature, and the reduction of voids and imperfections as a function of annealing temperature [24]. Furthermore, a blue shift occurs in the absorption edge (shift to higher energy) in the transmittance spectra, Fig. 6, with increased annealing temperature, which refers to an increase in the optical bandgap with an increase in annealing temperature. All the annealed films showed excellent optical properties that can be enhanced as a window layer in thin film solar cells applications [40].

The values of the absorption coefficient, α, as a function of the photon energy for as-prepared and annealed $(ZnSe)_{0.9}Cu_{0.1}$ thin films are shown in Fig. 7. It has been observed that the absorption coefficient decreases with increasing annealing temperature and photon energy, and it shifts to higher photon energy ($h\nu$). This may be due to the enhancement of crystallinity and a decrease in impurities at the grain boundaries with increasing annealing temperature [41], illustrating that the optical band gap, E_g^{opt}, of the examined films is influenced by annealing temperature.

However, the Tauc equation [42] can be used to determine the energy of the optical band gap in the high absorption region ($\alpha > 10^4$ cm^{-1}) for the films studied at various annealing temperatures:

$$\alpha h\nu = B(h\nu - E_g^{opt})^r \tag{20}$$

Where B is a constant related to the probability of transition, E_g^{opt} refer to the optical band gap energy, r s an exponent that corresponds to the kind of band-to-band transition that occurs in semiconductor materials; it is equal to $1/2$ for direct allowed transitions and 2 for indirect allowed transitions. The direct transition ($r = 1/2$) is revealed in the current work by the dependence of $(\alpha h\nu)$ as a function of the input photon energy.

By plotting $(\alpha h\nu)^2$ vs. photon energy $(h\nu)$ of the experimental data, the intercept of the fitted straight line to the axis of photon energy. The values of the direct optical band gap of $(ZnSe)_{0.9}Cu_{0.1}$ thin films with varying annealing

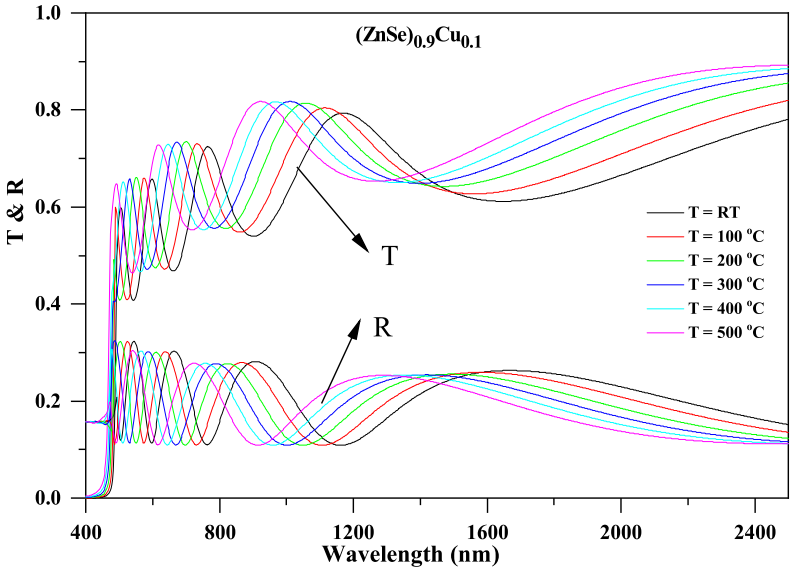

Fig. 6: The reflectance, R_λ, and transmittance, T_λ, spectra as a function of wavelength for as-prepared and differently annealed $(ZnSe)_{0.9}Cu_{0.1}$ thin films.

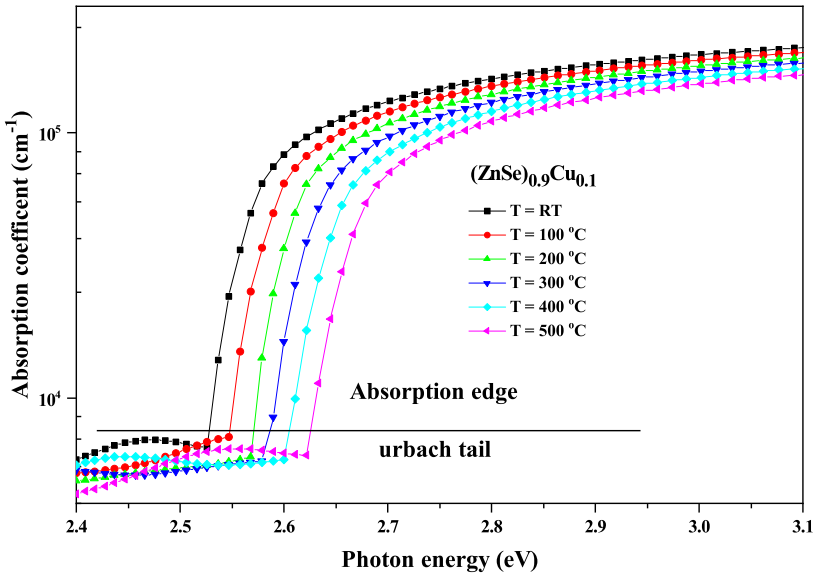

Fig. 7: The variations of the absorption coefficient, α, as a function of photon energy, $h\nu$, for as-prepared and annealed $(ZnSe)_{0.9}Cu_{0.1}$ thin films.

temperatures are obtained through the intercept of the fitted straight line to the axis of photon energy, as shown in Fig. 8, as the annealing temperatures rise from 100 °C to 500 °C, it has been found that the optical band gap magnitude of as-prepared and annealed $(ZnSe)_{0.9}Cu_{0.1}$ thin films varies between 2.527 and 2.659 eV. These films acquired an optical energy band gap that is less stretched and almost identical to the normal band gap (2.70 eV) of bulk ZnSe. This indicates that the optical band gap is dependent on the annealing temperatures. The increase in the optical band gap with increasing annealing temperature may be deduced by the Burstein–Moss Effect in semiconductors, which causes a blue shift of the absorption edge with increasing carrier concentration [43]. Additionally, as measured by XRD data analysis, higher annealing temperatures result in good crystallinity with a stable lattice structure and a decrease in dangling bonds, lattice

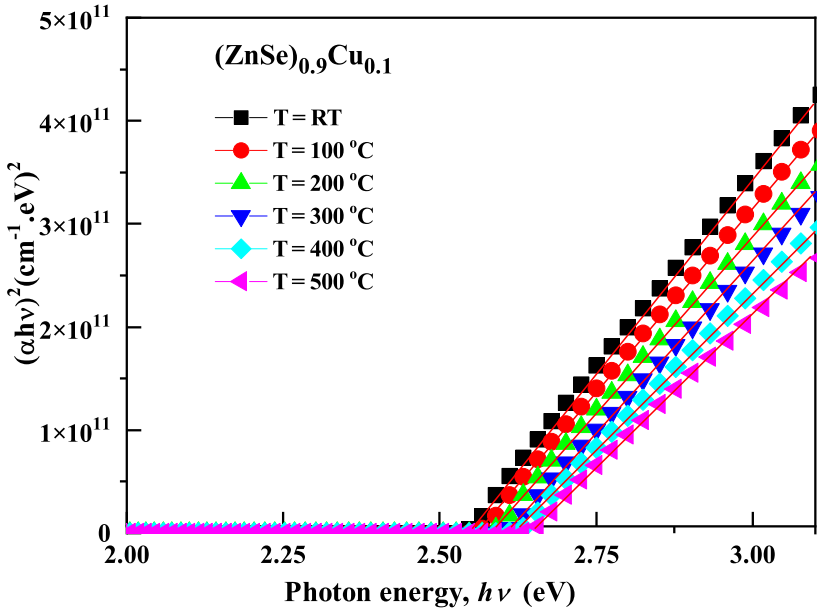

Fig. 8: Graphs of $(\alpha h\nu)^2$ vs. photon energy $(h\nu)$ for annealed $(ZnSe)_{0.9}Cu_{0.1}$ thin films.

strain, and dislocations that form around the surface of crystallites [44]. The behaviours of our study are in good agreement with the results obtained by the literature [45].

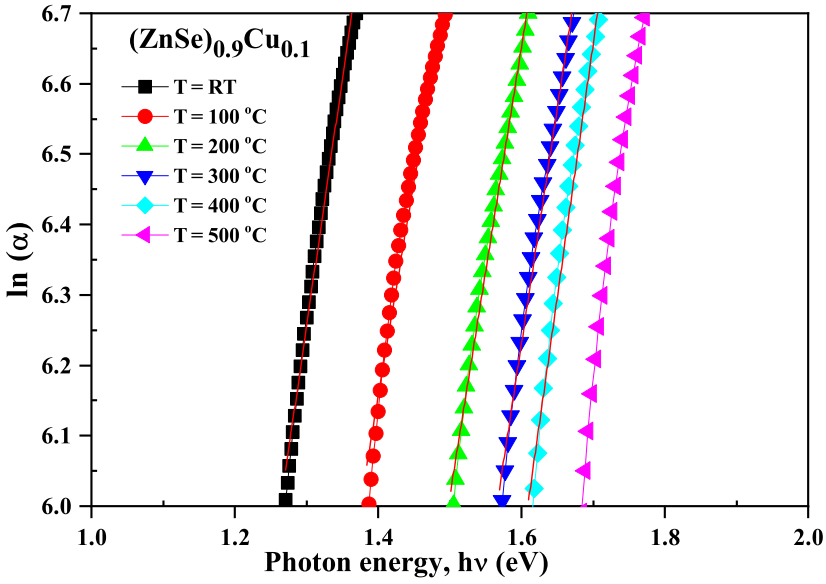

Fig. 9: $\ln(\alpha)$ as a function of photon energy $(h\nu)$ for as-prepared and annealed $(ZnSe)_{0.9}Cu_{0.1}$ thin films.

Applying Urbach's rules to evaluate the localized tail states in the band structure of the examined thin films with different annealing temperatures, by using the formula below [46].

$$\alpha(h\nu) = \alpha_0 \exp\left(\frac{h\nu}{E_e}\right) \tag{21}$$

Here, α_0 is a constant, and the slope of the plotting $\ln(\alpha)$ vs. photon energy $(h\nu)$. Figure 9 gives the localized tail state values for different investigated films. The estimated values of α_0 and localized tail state E_e with varying annealing temperatures are depicted in Fig. 10. It is observed that an inverse trend between α_0 and localized tail state E_e as the annealing temperatures increased. This could be clarified through a decrease in the dangling bond and defects in the lattice, causing an increase in the width of the localized tail states in the forbidden gap between the valence and conduction band structure. The relations between α_0 and E_e demonstrate the effect of annealing temperature on crystallization without breaking of more surface bonding between crystals. Furthermore, a significant drop of E_e at 100 °C refers to good distribution of nuclei and atoms during crystallization as described of decreasing the number of crystallites per unit area with decreasing defects in the lattice [31,34,35].

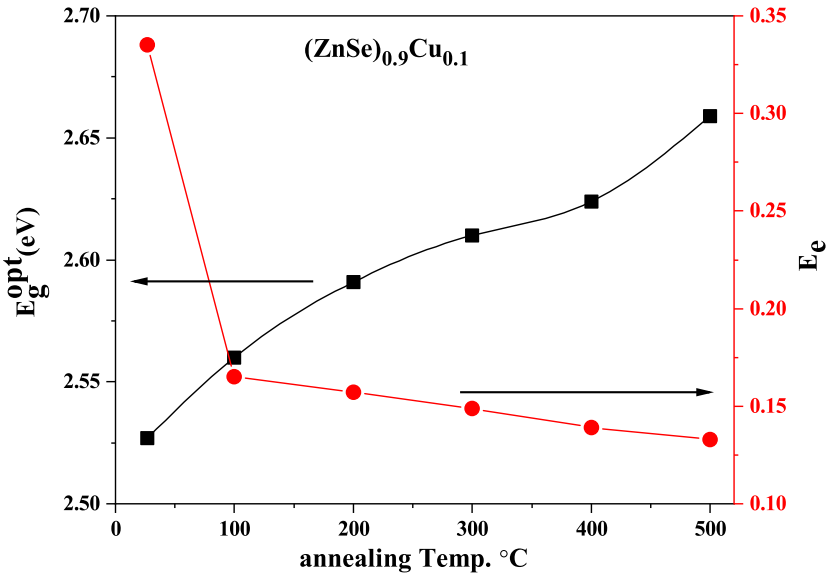

Fig. 10: Variations of the direct optical band gap E_g^{opt} versus localized tail state (E_e) as a function of annealed temperatures of $(ZnSe)_{0.9}Cu_{0.1}$ thin films.

3.2.2 Steepness parameters and electron phonon interactions

The steepness parameter, σ which indicates the strength of the absorption band broadening due to electron–phonon or exciton–phonon interactions, can be calculated from the following relation [47]

$$\sigma = \frac{k_B T}{E_e} \tag{22}$$

where k_B is the Boltzmann constant and T is the absolute temperature. Furthermore, another parameter related to steepness parameters is the electron–phonon interaction, which can be described as the relation below [48].

$$E_{e\to p} = \frac{2}{3}\sigma \tag{23}$$

Fig. 11 depicts the variation of steepness parameters and electron–phonon interactions as a function of annealing temperatures. One can notice that the steepness parameters increase while the electron–phonon interactions decrease with increasing annealing temperatures of thin films. This behaviour may be due to the increase in the degree of crystallinity with the decrease in localized states in the forbidden gap generated by impurities and imperfections [48,49]. These results are in good agreement with XRD microstructural analysis of the materials under investigation.

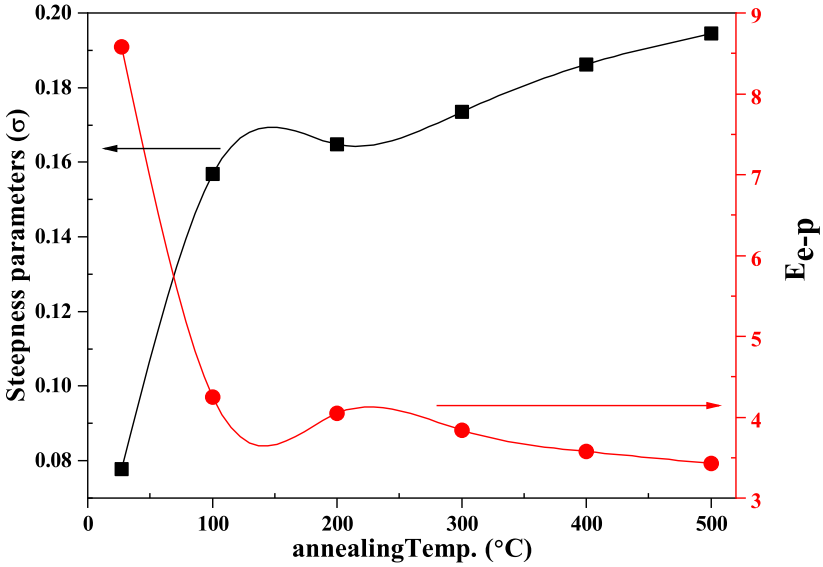

Fig. 11: Variation of both steepness parameter (σ) and electron–phonon interaction (E_{e-p}) of $(ZnSe)_{0.9}Cu_{0.1}$ thin films annealed at different temperatures.

3.2.3 Refractive index and extinction coefficient of thin films

Due to the electronic polarization and the materials' electric field confinement, the refractive index (n) is regarded as the most crucial property in semiconductor materials for optoelectronic devices. Using the Swanepoel formula for the envelope procedure mentioned below, the transmission spectra of the assessed films with different annealing temperatures are utilized to determine the fluctuation of the refractive index (n) [50].

$$n = \left[N + \sqrt{N_2 - S_2}\right]^{1/2} \tag{24}$$

and

$$N = 2s\frac{T_{Min} - T_{min}}{T_{Min}T_{min}} + \frac{s^2+1}{2}, \qquad s = \frac{1}{T_s} + \left(\frac{1}{T_s^2}\right)^{1/2} \tag{25}$$

where s is the substrate's refractive index, Fig. 12, refer to T_{Mass} , and T_{min} of the maxima and minima of the interference fringes in the transmittance spectra at the same fitted envelope wavelength, respectively. The variations in wavelength (λ) lead to alterations in the refractive index (n) in different annealing $(ZnSe_{0.9}Cu_{0.1}$ thin films as shown in Fig. 13. The estimated values of refractive index, n, decrease gradually as a function of increasing wavelength and annealing temperatures due to the dispersion behaviour of the materials. In addition, the initial sharp decrease of n with wavelength indicated a rapid change in the absorption energy of the material [51].

On the other hand, the dependence of the extinction coefficient, k, on the wavelength, λ, of as-prepared and annealed films is calculated from the formula described below and illustrated in Fig. 14 [29].

$$k = \frac{\alpha\lambda}{4\pi} \tag{26}$$

where, λ is the wavelength of the light incident. The extinction coefficient, k, at the values of wavelength close to 500 nm for all samples tends to zero. In contrast, in the range of wavelengths before 500 nm, the variations of the value of the extinction coefficient, k, decrease gradually with increasing wavelength for all thin films. This is because a decrease in absorbance and the fraction of incident light agree with the absorption coefficient, α [52]. In addition, the extinction coefficient, k, was decreasing with increasing annealing temperatures for all samples due to the blue shift of the absorption edge. The low extinction coefficient makes ZnSe films full of potential applications, such as in photo-detectors and solar cells [45].

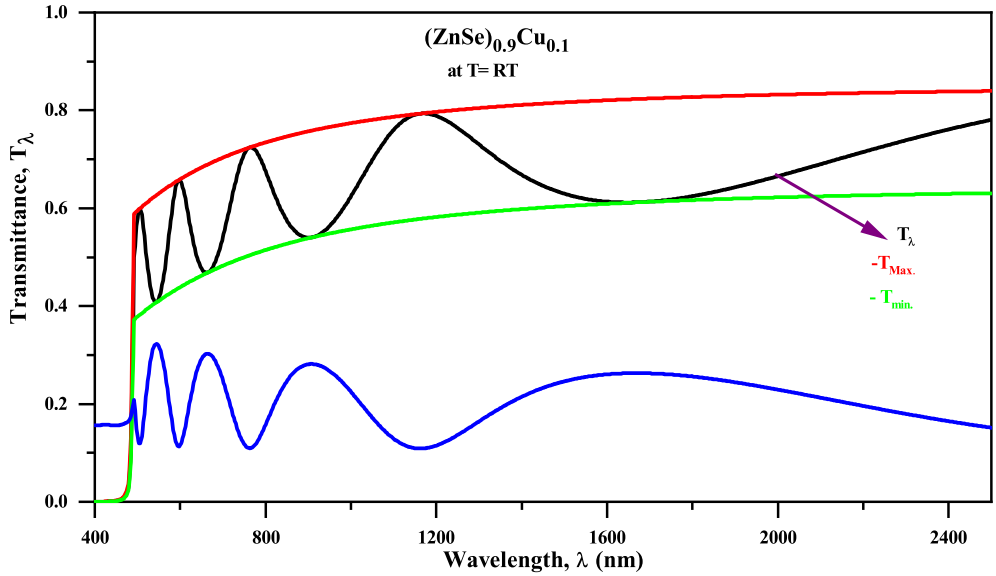

Fig. 12: transmittance spectra, T_λ, as a function of the wavelength of as-prepared $(ZnSe)_{0.9}Cu_{0.1}$ thin films.

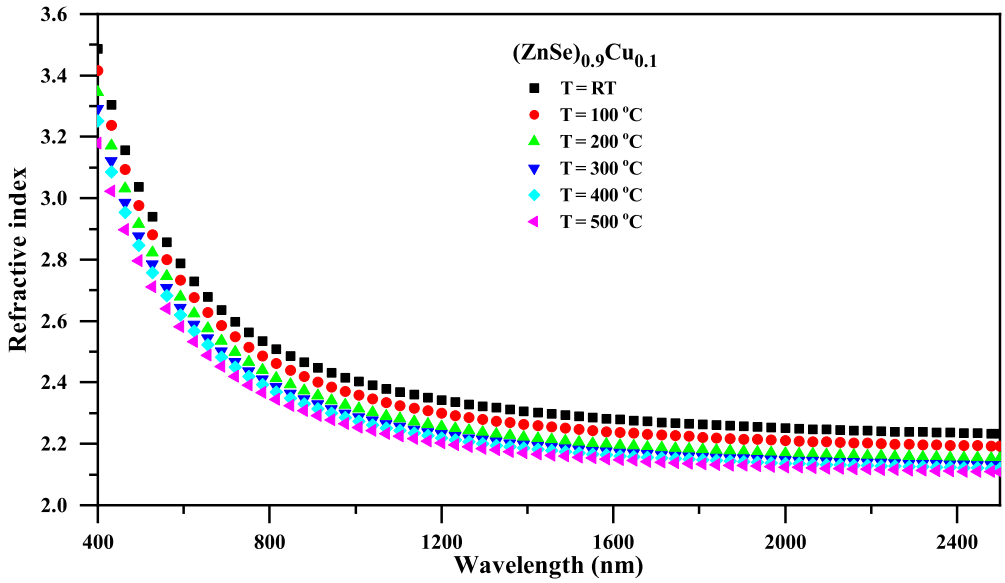

Fig. 13: The variations of refractive index (n) with wavelength (λ) of the studied $(ZnSe)_{0.9}Cu_{0.1}$ thin films.

3.2.4 Dielectric constants, loss factor, and optical electronegativity

Numerous factors for electrical applications of semiconducting materials are directly influenced by the dielectric characteristics, which are further impacted by the material's electronic parameters. The band gap, which is altered by electromagnetic radiation passing through the film, determines the dielectric property. The dielectric constant, $(\varepsilon = \varepsilon_r + i\varepsilon_i)$, is a significant property of the material that is related to n and k, the real parts $\varepsilon_r = n^2 - k^2$ demonstrate the inadequate of energy or the incorporate light, while the imaginary parts $\varepsilon_i = 2nk$ known the damping factor, which related to dissipative rate of energy through the propagation into the films and dissipation factor that is the ratio of the imaginary and real part $\tan\delta = \varepsilon_i/\varepsilon_r$ [53]. The ε_r, ε_i, and $\tan\delta$ are estimated for $(ZnSe)_{0.9}Cu_{0.1}$ thin films annealed at different temperatures, plotted as a function of wavelength and annealing temperature, as shown in Fig. 15(a,b and c).

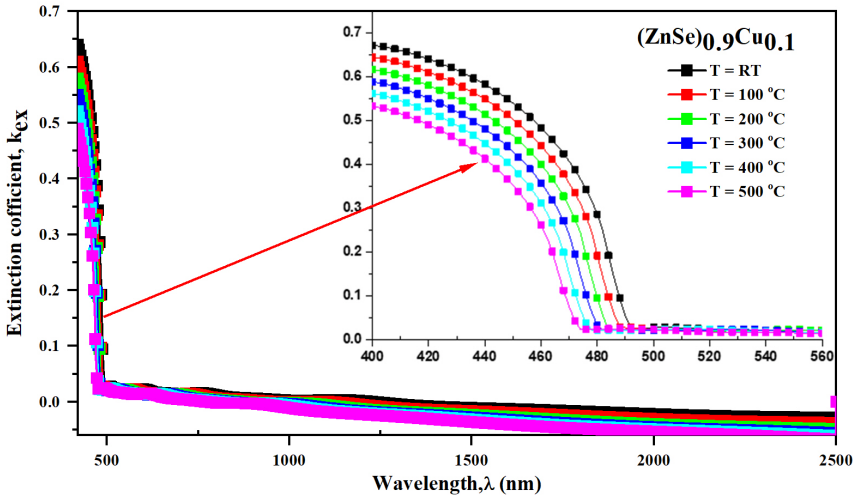

Fig. 14: Extinction coefficient (k) versus wavelength (λ) of the studied $(ZnSe)_{0.9}Cu_{0.1}$ thin films.

The results collected show that the values of ε_r are higher than those of ε_i and decrease gradually for all samples with annealing temperatures.

To comprehend how energy absorption is lost and slowed down during single-electron transitions or the collective effects generated in the material, two further essential features are required (VELF) and (SELF). The real, ε_r, and imaginary, ε_i, components of the dielectric constants are connected to the volume energy (VELF) and surface energy loss functions (SELF), respectively, and are inferred using the following equations [54,55].

$$\text{VELF} = \frac{\varepsilon_2}{\varepsilon_1^2 + \varepsilon_2^2}, \qquad \text{SELF} = \frac{\varepsilon_2}{(\varepsilon_1 + 1)^2 + \varepsilon_2^2} \tag{27}$$

The association between the photon energy, $h\nu$, and the changes in the volume and surface energy loss functions (VELF and SELF) for $(ZnSe)_{0.9}Cu_{0.1}$ thin films is illustrated in Fig. 16(a and b). It is evident that the values of functions VELF and SELF, respectively, increase as the photon energy, $h\nu$, increases, and that they decrease as the annealing temperature increases. On the other hand, optical electronegativity (η_{opt}) is the capacity of the positive radicals of atoms of any material to attract electrons to create ionic bonds. The equation can be used to estimate it for any solid material [56].

$$\eta_{\text{opt}} = \left(\frac{C}{n_0}\right)^{1/4} \tag{28}$$

where $C = 25.54$ is a constant. The calculated value of optical electronegativity is listed in Table 4, and increases as a function of annealing temperature.

$$\eta_{\text{opt}} = \left(\frac{C}{n_0}\right)^{1/4} \tag{28}$$

whereas $C = 25.54$ is a constant. The calculated value of optical negativity is listed in table 4, and increases as a function of annealing temperature.

In order to identify optoelectronic materials based on refractive index dispersion properties, the dispersion energy is crucial, which can be evaluated using a single oscillator Wemple-DiDomenico model described in the form [57].

$$n^2 = 1 + \frac{E_o E_d}{E_o^2 - E^2} \tag{29}$$

where E_d is the dispersion energy according to the interband optical transition, E_o is the single oscillator energy, and E is the photon energy. Based on the experimental data by graphing the refractive index factor $(n^2-1)^{-1}$ vs. $(h\nu)^2$ and fitting it with a straight line, the values of E_d and E_o are directly determined using the slope of the straight line $(1/E_d E_o)$ and the intercept at the Y-axis (E_o/E_d), respectively, as shown in Fig. 17.

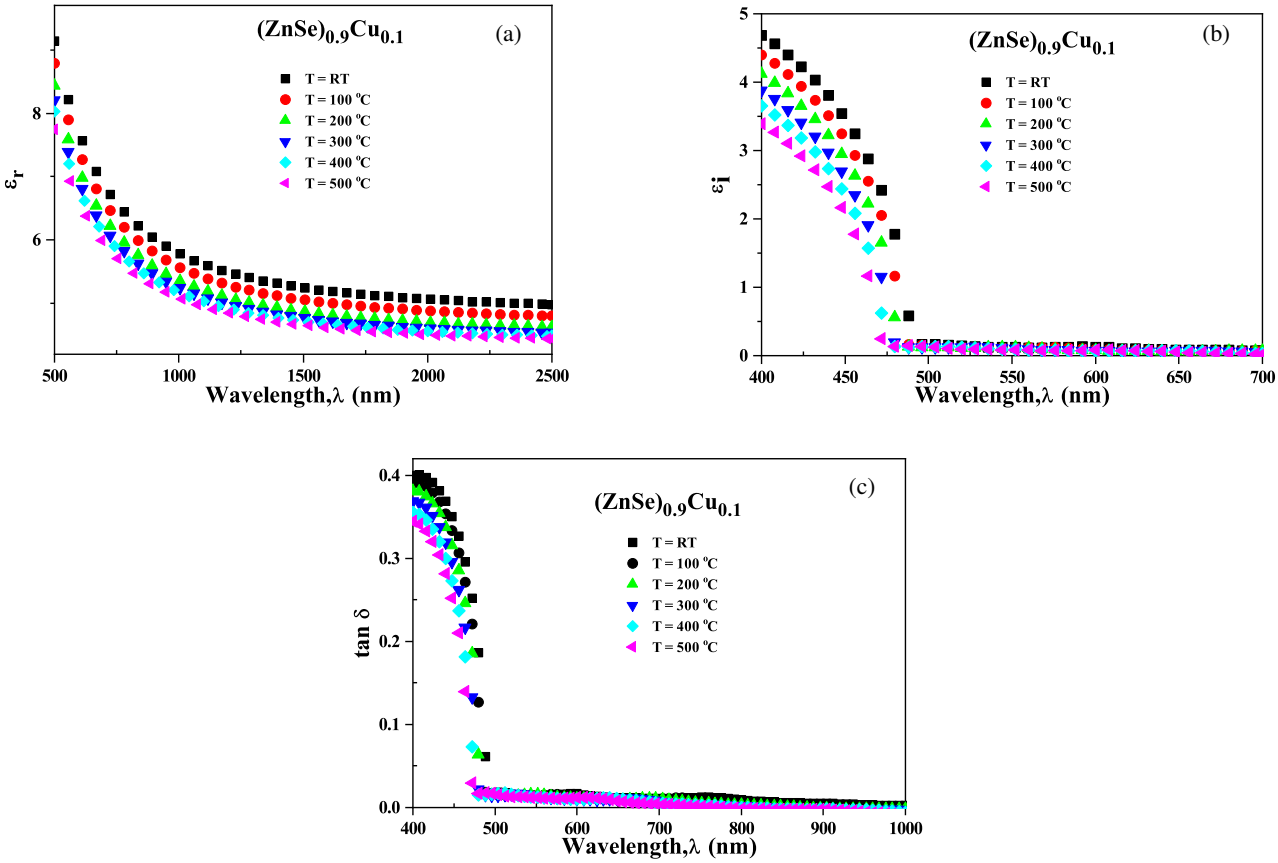

Fig. 15: Plots of real (a), imaginary (b) parts of the dielectric constants and dissipation factor tan δ (c) as a function of the wavelength, λ, of annealed $(ZnSe)_{0.9}Cu_{0.1}$ thin films.

The values E_o and E_d of as-prepared and annealed films are designated in table 4. It has been noted that, as the annealing temperature increases, the values of single oscillator energy E_o decrease until the annealing temperature reaches 200°C; after that, the values of E_o increase with increasing annealing temperatures. While the dispersion energy E_d decreases gradually as a function of annealing temperatures. The changes in single oscillator energy E_o with an increase in annealing temperatures are associated with the blue shift that occurs in films with increasing annealing temperatures. In addition, the decrease in defects and atomic migration with increasing annealing temperatures leads to a good crystallization rate, which causes a decrease in E_d [45]. The two optical parameters that are related to single oscillator energy (E_o) and dispersion energy (E_d) are the moments of the optical spectrum (M-1 and M-3) that can be deduced from the equation [58].

$$M_{-1} = \frac{E_d}{E_o}, \quad M_{-3} = \frac{M_{-1}}{E_o^2} \tag{30}$$

As shown in table 4, the estimated values of M-1 and M-3 decrease with increasing annealing temperatures. Furthermore, as illustrated in Fig. 18, the high-frequency dielectric constant, ε_r, is derived from the plot of the square of the wavelength, λ^2, against the square of the refractive index, n^2, and is associated with the concentration of free carriers. The following equation states that the dielectric constant of a real section at high frequencies was found using the intercept of a vertical axis [58].

$$n^2 = \varepsilon_r - \frac{e^2 N}{4\pi c^2 \varepsilon_0 m^*}\lambda^2 \tag{31}$$

where (N/m^*) is the conduction band free carrier concentration to the free carrier effective mass, e is the electron's charge, c is the light velocity, and ε_0 is the vacuum permittivity. Figure 18 shows that the intercept of the linear part at $\lambda^2 = 0$

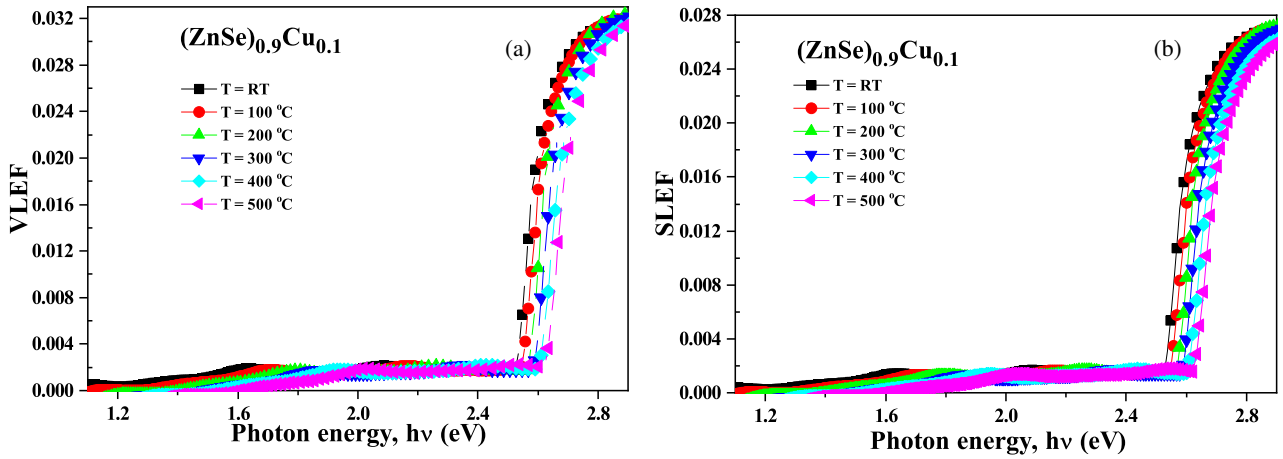

Fig. 16: (a) VELF and (b) SELF versus photon energy ($h\nu$) of annealed $(ZnSe)_{0.9}Cu_{0.1}$ thin films.

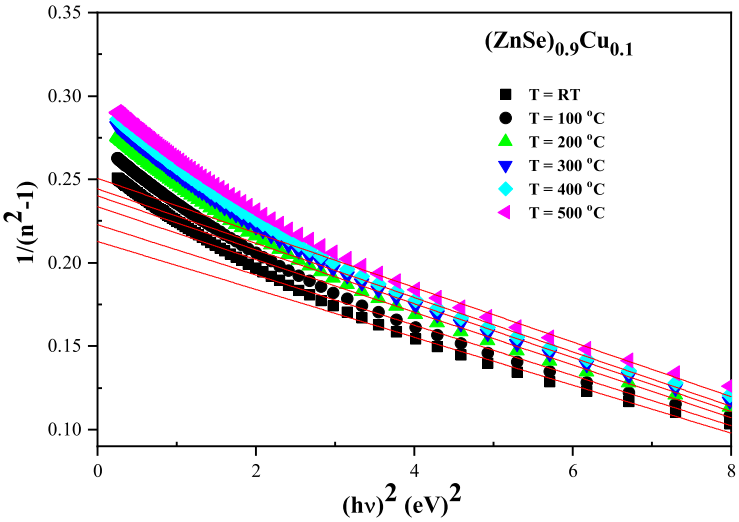

Fig. 17: Graph of $(n^2-1)^{-1}$ vs. $(h\nu)^2$ of $(ZnSe)_{0.9}Cu_{0.1}$ thin films annealed at different temperatures.

approaches the value of the lattice dielectric constant, ε_r. While the ratio of free carrier concentration (N/m^*) is computed from the gradient of the straight line, the values are calculated and listed in table 4. The static refractive index, n_0, is related to the model of dispersion energy at the value of $(h\nu = 0)$ and a single oscillator. Then, it is calculated according to the equation [57].

$$n_0 = \sqrt{1 + \frac{E_d}{E_o}} \tag{32}$$

where, $\varepsilon_i = n_0^2$ is named the zero frequency dielectric constant. As a result, the calculated values of n_0, ε_r, (N/m^*), and ε_i of $(ZnSe)_{0.9}Cu_{0.1}$ thin films annealed at different temperatures decrease with an increase in the annealing temperatures, which can be related to the internal microstructure of materials under investigation [59].

The average interband oscillator wavelength (λ_0) and average oscillator strength (S_0) for each film under investigation with a distinct refractive index can be determined by further examining the refractive index n. The following equation describes the single Sellmeier oscillator equation at low energies [60].

$$\frac{n_\infty^2 - 1}{n^2 - 1} = 1 - \left(\frac{\lambda_0}{\lambda}\right)^2 \tag{33}$$

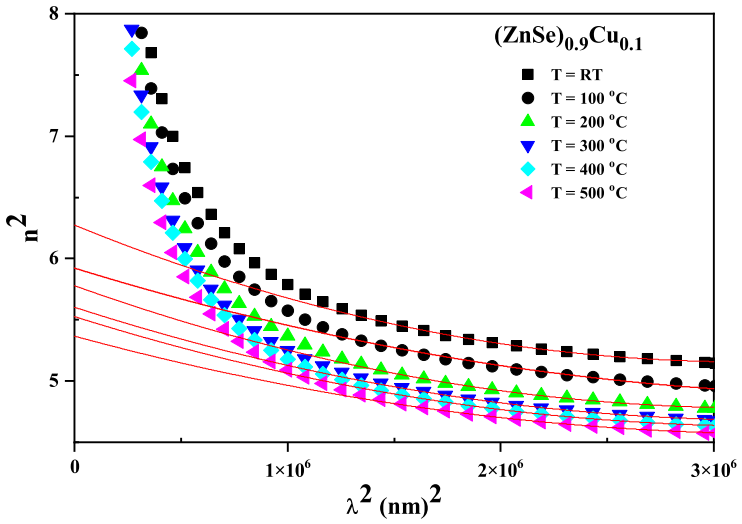

Fig. 18: Variations of n^2 vs. λ^2 of $(ZnSe)_{0.9}Cu_{0.1}$ thin films annealed at different temperatures.

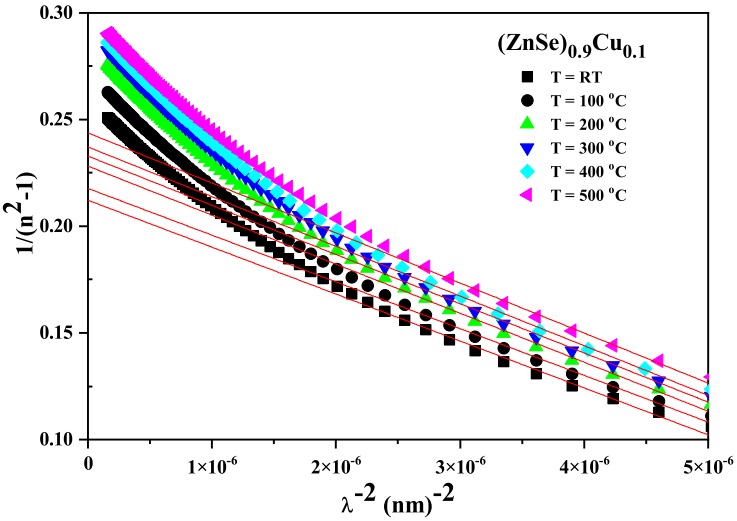

Fig. 19: Variations of n^2 vs. λ^2 of $(ZnSe)_{0.9}Cu_{0.1}$ thin films annealed at different temperatures.

where n_∞ is the empty lattice's refractive index at an infinite wavelength. By graphing $(n^2-1)^{-1}$ vs. λ^{-2}, as seen in Fig. 19, the slope and intercept of a straight line were used to calculate the parameters (λ_0) and (S_0), respectively, of $(ZnSe)_{0.9}Cu_{0.1}$ of as-prepared and annealed films. The obtained values of S_0 and λ_0 are tabulated in Table 4 and decrease with increasing annealing temperatures.

Conversely, Drude's hypothesis posits that the carrier concentration of the material is associated with the plasma frequency (ω_p) through the following equation:

$$\omega_p^2 = \frac{e^2}{\varepsilon_r \varepsilon_0}\left(\frac{N}{m^*}\right) \tag{26}$$

where ε_0 represents the dielectric permittivity of vacuum (8.854×10^{-12} F/m), while e denotes the charge of an electron. The values of ω_p were calculated and listed in Table 4. The calculated values of ω_p illustrate an increase in values compared with the estimated values indicated at room temperature. Furthermore, as the annealing temperature increases,

the plasma frequency decreases gradually. These results indicate dependence of dispersion parameters on annealing temperatures and the degree of crystallinity in the material.

Table 4: Calculated some of the optical parameters of the polycrystalline $(ZnSe)_{0.9}Cu_{0.1}$ thin films annealed at different temperatures.

Optical Parameters	**RT**	**100**	**200**	**300**	**400**	**500**
Dispersion energy, E_d (eV)	15.98	16.98	16.01	15.76	15.63	15.24
Oscillator energy, E_o (eV)	3.858	3.82	3.807	3.824	3.855	3.872
First moments of optical spectra (M-1)	4.141	4.444	4.227	4.120	4.054	3.937
Second moments of optical spectra (M-3)	0.278	0.305	0.292	0.282	0.273	0.263
Static refractive index, n_0	2.267	2.333	2.286	2.263	2.248	2.222
High-frequency dielectric constant, ε_r	6.25	5.92	5.77	5.60	5.51	5.36
Static linear dielectric constant, ε_i	5.141	5.443	5.226	5.121	5.054	4.937
Carrier concentration $(N/m^* \times 10^{43}\,\mathrm{Kg^{-1}m^{-3}})$	3.83	9.20	8.14	7.86	7.34	6.575
Oscillator strength $S_0 \times 10^{13}\,\mathrm{m^2}$	2.07	3.485	3.375	3.116	3.278	3.243
Oscillator wavelength, λ_0 (nm)	407.9	347.37	346	351.61	342.96	340.16
Plasma frequency, $\omega_p \times 10^{15}$ Hz	4.44	11.96	10.99	10.85	10.28	9.41
Optical electronegativity, η_{opt}	1.832	1.819	1.828	1.833	1.836	1.841

3.3 Non-linear optical analysis

When a nonlinear medium interacts with an electric field, the polarization associated with the field is also nonlinear. A high-intensity electric field affects many parameters, such as bond length, electron polarizability, and nuclear interaction, when incident on thin films, which are dependent on nonlinear properties in chalcogenide thin films. The first non-linear susceptibility, third-order ($\chi^{(1)}$), ($\chi^{(3)}$) and non-linear refractive index (n_2) respectively can be obtained according to the following [61,62].

$$\chi^{(1)} = \frac{E_d}{4\pi E_o} \tag{35}$$

$$\chi^{(3)} = \frac{A(n_0^2-1)^4}{(4\pi)^4} \tag{36}$$

Here, $A = 1.79 \times 10^{-10}$ esu.

$$n_2 = \frac{12\pi\chi^{(3)}}{n_0} \tag{37}$$

The calculated values of the first- and third-order non-linear susceptibility ($\chi^{(1)}$, $\chi^{(3)}$) and non-linear refractive index (n_2) as a function of annealing temperatures are summarized in table 5. The present results reveal that the non-linear optical parameters are affected by annealing temperatures and decrease with increasing annealing temperatures. This behavior agrees with some reported studies [56,63]. The chalcogenide materials have higher values of non-linear susceptibility compared with the estimated values of oxide glasses. In addition, self-refraction is indicated by a non-linear refractive index. Materials having a non-linear refractive index greater than zero indicate a particular behavior due to periodic self-focusing rather than diffraction in the glass when the incident beam transfers through the medium. The results of the investigated materials refer to the materials that are used in many nonlinear optics applications with good efficiency, such as photonics, optical switching, and various optoelectronic applications [56].

Table 5: Non-linear optical parameters of annealed $(ZnSe)_{0.9}Cu_{0.1}$ thin films.

Temp. (C°)	$\chi^{(1)}$ (esu)	$\chi^{(3)} \times 10^{-12}$ (esu)	$n_2 \times 10^{-11}$ (esu)
RT	0.33	2.043	3.409
100	0.353	2.779	4.496
200	0.336	2.281	3.762
300	0.328	2.071	3.450
400	0.322	1.924	3.227
500	0.313	1.718	2.915

4 Conclusions

The present report refers to $(ZnSe)_{0.9}Cu_{0.1}$ chalcogenide thin films that were deposited using the thermal evaporation technique and annealed in the temperature range from 100°C to 500°C. XRD diffraction indicates a unique wurtzite phase of ZnSe nanocrystalline with no appearance of other phases with increasing annealing temperatures. The microstructural properties showed that the degree of crystallinity and average crystallite size increased, while the lattice strain and dislocation density decreased. Other microstructural parameters such as Lorentz factor, number of crystallites per unit surface, bond length, and bond angles, are related to annealing temperatures.

The optical properties refer to a decrease in transmittance and absorption coefficient as a function of annealing temperatures. In addition, the direct optical band gap increases from 2.632 to 2.527 eV with a blue shift of the absorption edge, while the Urbach energy decreases from 2.632 to 2.527 eV. The annealing temperatures are also influential on steepness parameters, electron-phonon interaction, refractive index n, and extinction coefficient k_{ex}. Further, the dielectric constant, loss factor, dispersion parameters, and the non-linear optical parameters are sensitive to the annealing temperatures. The changes in linear and nonlinear optical properties of the investigated thin films are useful and enhance many optoelectronic devices and applications.

Conflict of Interest

The authors declare that there is no conflict of interest regarding the publication of this paper.

References

[1] J. Hu, X. Sun, A. M. Agarwal, J.-F. Viens, L. C. Kimerling, L. Petit, N. Carlie, K. C. Richardson, T. Anderson and J. J. Choi, Studies on structural, electrical, and optical properties of Cu doped As–Se–Te chalcogenide glasses, *Journal of Applied Physics* **101** (2007) p. 063520.

[2] M. M. Khan, M. W. Khan, M. Husain and M. J. Zulfequar, Electrical transport and optical properties of Zn doped Bi–Se chalcogenide glasses, *Journal of Alloys and Compounds* **486** (2009) 876–880.

[3] Y. T. Alharbi, Synthesis and characterization of Mn_4S_4:Ni_2S_2 chalcogenide electrodes for superior supercapacitive properties, *University of Bisha Journal for Basic and Applied Sciences* **2** (2026) 22–33.

[4] D. Souri, A. R. Khezripour, M. Molaei and M. J. Karimipour, ZnSe and copper-doped ZnSe nanocrystals, *Current Applied Physics* **17** (2017) 41–46.

[5] M. A. Sayeed, H. K. Rouf and K. M. A. Hussain, Effect of thickness on characteristics of ZnSe thin film synthesized by vacuum thermal evaporation, *Journal of Theoretical and Applied Physics* **14** (2020) 251–259.

[6] L. Ezenwaka, N. Okoli, N. Okereke, I. Ezenwa and N. J. Nwori, Properties of electrosynthesized cobalt doped zinc selenide thin films, *Nanoarchitectonics* **3** (2021) 1–9.

[7] M. Ashraf, S. Akhtar, A. Khan, Z. Ali and A. J. Qayyum, Effect of annealing on structural and optoelectronic properties of nanostructured ZnSe thin films, *Journal of Alloys and Compounds* **509** (2011) 2414–2419.

[8] B. Güzeldir, M. Sağlam and A. J. Ateş, Electrical characteristics of Zn/ZnSe/n-Si/Au–Sb structure, *Journal of Alloys and Compounds* **506** (2010) 388–394.

[9] A. Othonos, E. Lioudakis, D. Tsokkou, U. Philipose and H. E. Ruda, Ultrafast time-resolved spectroscopy of ZnSe nanowires, *Journal of Alloys and Compounds* **483** (2009) 600–603.

[10] S. Li, L. Wang, X. Su, Y. Pan, D. Gao and X. Han, Optical properties of co-doped ZnSe thin films, *Thin Solid Films* **692** (2019) p. 137599.

[11] Z. B. Bahşi and A. Y. Oral, Effects of Mn and Cu doping on the microstructures and optical properties of ZnO thin films, *Optical Materials* **29** (2007) 672–678.

[12] C. Coughlan, M. Ibanez, O. Dobrozhan, A. Singh, A. Cabot and K. M. Ryan, Compound copper chalcogenide nanocrystals, *Chemical reviews* **117**(9) (2017) 5865–6109.
[13] F. Yao, X. Zhou and A. Xiong, Tunable electronic and optical properties of two-dimensional ZnSe/AlAs van der waals heterostructure, *Applied Physics A* **126** (2020) 1–10.
[14] F. Long, S. Ning, W. Zhang, S. Wang, H. Yang, H. Zhang, G. Feng and S. Zhou, All-fiber passively q-switched erbium-doped laser with Cr2+: ZnSe nanocrystals saturable absorber, *Laser Physics* **30** (2020) p. 055101.
[15] M. El Sherif, F. Terra and S. Khodier, Optical characteristics of thin ZnSe films of different thicknesses, *Journal of Materials Science: Materials in Electronics* **7** (1996) 391–395.
[16] W. Daranfed, M. S. Aida, N. Attaf, J. Bougdira and H. Rinnert, Cu_2ZnSnS_4 thin films deposition by ultrasonic spray pyrolysis, *Journal of Alloys and Compounds* **542** (2012) 22–27.
[17] A. Rumberg, C. Sommerhalter, M. Toplak, A. Jäger-Waldau and M. C. Lux-Steiner, ZnSe thin films grown by chemical vapour deposition for application as buffer layer in CIGSS solar cells, *Thin Solid Films* **361** (2000) 172–176.
[18] J.-S. Seol, S.-Y. Lee, J.-C. Lee, H.-D. Nam and K.-H. Kim, Electrical and optical properties of Cu_2ZnSnS_4 thin films prepared by rf magnetron sputtering process, *Solar Energy Materials and Solar Cells* **75** (2003) 155–162.
[19] E. Bacaksiz, S. Aksu, I. Polat, S. Yılmaz and M. Altunbaş, The influence of substrate temperature on the morphology, optical and electrical properties of thermal-evaporated ZnSe thin films, *Journal of Alloys and Compounds* **487** (2009) 280–285.
[20] M. N. Abdel-Salam, N. Sabry, E. S. Yousef and E. R. Shaaban, Effect of Cu ratios dopant on ZnSe thin films structural and optical properties, *Chalcogenide Letters* **20** (2023) 759–777.
[21] S. Adachi, *Properties of semiconductor alloys: group-IV, III-V and II-VI semiconductors* (John Wiley & Sons, 2009).
[22] S. S. Kumar, A. Sharma, G. M. Rao and S. J. Suwas, Investigations on the effect of substrate temperature on reactively sputtered zirconium carbide thin films, *Journal of Alloys and Compounds* **695** (2017) 1020–1028.
[23] S. Mahato and A. J. Kar, Structural, optical and electrical properties of electrodeposited cadmium selenide thin films, *Journal of Electroanalytical Chemistry* **742** (2015) 23–29.
[24] H. N. Rosly, K. S. Rahman, M. N. Harif, C. Doroody, M. Isah, H. Misran and N. J. S. Amin, Annealing temperature assisted microstructural and optoelectrical properties of CdSe thin film, *Superlattices and Microstructures* **148** (2020) p. 106716.
[25] N. J. Gregory, Elements of X-ray diffraction, *Journal of the American Chemical Society* **79** (1957) 1773–1774.
[26] M. N. H. Mia, M. F. Pervez, M. K. Hossain, M. R. Rahman, M. J. Uddin, M. A. Al Mashud, H. K. Ghosh and M. J. R. Hoq, Influence of Mg content on tailoring optical bandgap of Mg-doped ZnO thin film, *Results in Physics* **7** (2017) 2683–2691.
[27] D. P. Padiyan and A. J. Marikani, X-ray determination of lattice constants of $CdXSn_{1-x}Se$ mixed crystal systems, *Crystal Research and Technology* **37** (2002) 1241–1248.
[28] R. D. Shannon, Revised effective ionic radii and systematic studies of interatomic distances, *Foundations of Crystallography* **32** (1976) 751–767.
[29] A. Purohit, S. Chander, S. Nehra, C. Lal and M. J. Dhaka, Effect of thickness on nanocrystalline CdSe thin films, *Optical Materials* **47** (2015) 345–353.
[30] I. J. El Radaf, Structural and optoelectrical characterization of $Cu_2ZnGeSe_4$ thin films, *Journal of Materials Science: Materials in Electronics* **31** (2020) 3228–3237.
[31] C. V. Thompson, Grain growth in thin films, *Annual Review of Materials Science* **20** (1990) 245–268.
[32] D. Suthar, G. Chasta, S. Patel, S. Chander, M. Kannan and M. J. Dhaka, Impact of annealing conditions on ZnSe thin films, *Materials Research Bulletin* **132** (2020) p. 110982.
[33] G. Gottstein and L. S. Shvindlerman, *Grain boundary migration in metals* (CRC Press, 2009).
[34] F. J. Humphreys and M. Hatherly, *Recrystallization and related annealing phenomena* (Elsevier, 2012).
[35] W. W. Mullins, Two-dimensional motion of idealized grain boundaries, *Journal of Applied Physics* **27** (1956) 900–904.
[36] X. Wang, Z. Wu, J. Webb and Z. Liu, Ferroelectric and dielectric properties of Li-doped ZnO thin films, *Applied Physics A* **77** (2003) 561–565.
[37] L. B. Chandrasekar, R. Chandramohan, S. Chandrasekaran, J. Thirumalai and R. Vijayalakshmi, Luminescence and unit cell analysis of $Zn_{1-x}Cd_xO$ nanoparticles, *Advanced Science Focus* **1** (2013) p. 292.
[38] J. Joannopoulos and M. L. Cohen, Theory of short-range order and disorder in tetrahedrally bonded semiconductors, *Solid State Physics* **31** (1976) 71–148.
[39] R. Vahalová, L. Tichý, M. Vlček and H. J. Ticha, Far infrared spectra and bonding arrangement in Ge–Sb–S glasses, *physica status solidi (a)* **181** (2000) 199–209.
[40] C. Li, F. Wang, Y. Chen, L. Wu, J. Zhang, W. Li, X. He, B. Li and L. J. Feng, Characterization of sputtered CdSe thin films, *Materials Science in Semiconductor Processing* **83** (2018) 89–95.
[41] G. I. Rusu, M. Diciu, C. Pîrghie and E. J. Popa, Structural characterization and optical properties of ZnSe thin films, *Applied Surface Science* **253** (2007) 9500–9505.
[42] J. Tauc, *Amorphous and liquid semiconductors* (Springer, 2012).
[43] H. Sharma, S. N. Sharma, G. Singh and S. J. Shivaprasad, Effect of Cd:Se ratios on CdSe nanoparticles, *Physica E* **31** (2006) 180–186.
[44] E. J. Shaaban, Microstructure parameters and optical properties of cadmium ferrite thin films, *Applied Physics A* **115** (2014) 919–925.
[45] K. Ou, S. Wang, L. Bai, Y. Wang, K. Zhang and L. J. Yi, Annealing temperature dependent optical properties of ZnSe thin films, *Thin Solid Films* **669** (2019) 247–252.

[46] F. Urbach, The long-wavelength edge of electronic absorption, *Physical Review* **92** (1953) p. 1324.
[47] M. Mahesha, N. Meghana and M. J. Padiyar, Effect of annealing on thermally evaporated ZnSe thin films, *Physica B* **520** (2017) 37–42.
[48] J. Singh, V. Verma and R. Kumar, Influence of Mg substitution on optical band gap, *Results in Physics* **13** (2019) p. 102106.
[49] R. Vettumperumal, S. Kalyanaraman, B. Santoshkumar and R. J. Thangavel, Estimation of electron–phonon coupling and urbach energy, *Materials Research Bulletin* **77** (2016) 101–110.
[50] M. Mohamed, E. Shaaban, M. N. Abd-el Salam, A. Abdel-Latief, S. A. Mahmoud and M. J. Abdel-Rahim, Optical and electrical parameters of As–Se–Ag thin films, *Optik* **178** (2019) 1302–1312.
[51] N. Revathi, P. Prathap and K. T. R. Reddy, Thickness dependent physical properties of In_2S_3 films, *Solid State Sciences* **11** (2009) 1288–1296.
[52] O. El-Shazly, H. M. Khalifa, A. Sweyllam, F. F. El-Sanabary and E. F. El-Wahidy, Optical properties of Se–Te–Sb thin films, *Canadian Journal of Physics* **92**(4) (2014) 328–334.
[53] N. A. Bakr, A. Funde, V. Waman, M. Kamble, R. Hawaldar, D. Amalnerkar, S. Gosavi and S. Jadkar, Determination of optical parameters of a-Si:H thin films, *Pramana* **76** (2011) 519–531.
[54] M. Mohamed, A. Abdelraheem, M. Abd-Elrahman, N. Hadia and E. Shaaban, Composition dependence of optical properties of $CdS_{1-x}Mn_x$ thin films, *Applied Physics A* **125** (2019) p. 483.
[55] S. Wemple, Refractive-index behavior of amorphous semiconductors, *Physical Review B* **7** (1973) p. 3767.
[56] S. Das, D. Alagarasan, S. Varadharajaperumal, R. Ganesan and R. J. M. A. Naik, Nonlinear susceptibility of Ag–Se–Te nanostructured films, *Materials Advances* **3** (2022) 7640–7654.
[57] M. El-Nahass, M. Emam-Ismail and M. El-Hagary, Structural, optical and dispersion energy parameters of nickel oxide nanocrystalline thin films prepared by electron beam deposition technique, *Journal of Alloys and Compounds* **646** (2015) 937–945.
[58] A. S. Hassanien and I. J. Sharma, Optical properties of quaternary chalcogenide thin films, *Optik* **200** (2020) p. 163415.
[59] H. Nyakotyo, T. Sathiaraj, E. J. Muchuweni and L. Technology, Optical properties of amorphous Se–Te–Sb–Bi thin films, *Optics & Laser Technology* **92** (2017) 182–188.
[60] M. El-Hagary, M. Emam-Ismail, E. Shaaban, A. Al-Rashidi and S. J. M. C. P. Althoyaib, Structural and optical studies on $Zn_{1-x}Mn_xS$ thin films, *Materials Chemistry and Physics* **132** (2012) 581–590.
[61] H. Ticha and L. Tichy, Semiempirical relation between nonlinear susceptibility and optical gap, *Journal of Optoelectronics and Advanced Materials* **4** (2002) 381–386.
[62] E. R. Shaaban, M. Mohamed, M. N. Abd-el Salam, A. Y. Abdel-Latief, M. A. Abdel-Rahim and E. S. Yousef, Optical properties of annealed As–Se–Ag thin films, *Optical Materials* **86** (2018) 318–325.
[63] M. El-Nahass, H. Zeyada, N. El-Ghamaz and A. Shetiwy, Particle size reduction of thallium indium disulphide thin films, *Optik* **171** (2018) 580–588.